Hindawi
Scientific Programming
Volume 2022, Article ID 2656706, 11 pages
https://doi.org/10.1155/2022/2656706

Research Article

Curative Effect of Interventional Therapy and Neurological Changes in Ischemic Stroke of Posterior Circulation Evaluated by Magnetic Resonance Imaging under Genetic Algorithm

Xiaodu Yu,[1] **Xingyou Zheng**,[2] **and Daoyou Cheng**[3]

[1]*Department of Interventional Therapy, Affiliated Changsha Hospital of Hunan Normal University, Changsha 410006, Hunan, China*
[2]*Department of Radiology, Affiliated Changsha Hospital of Hunan Normal University, Changsha 410006, Hunan, China*
[3]*Department of Neurology, Xingyi Hospital Affiliated to Guizhou Medical University, Xingyi 562400, Guizhou, China*

Correspondence should be addressed to Daoyou Cheng; 3115307115@m.fafu.edu.cn

Received 27 September 2021; Revised 25 November 2021; Accepted 27 November 2021; Published 7 January 2022

Academic Editor: M Pallikonda Rajasekaran

Objective. This study aimed to evaluate the improvement and neurological function changes of patients with ischemic stroke in the posterior circulation before and after interventional therapy using magnetic resonance imaging (MRI) under genetic algorithm and compressed sensing algorithm. *Methods*. Thirty-six patients with posterior circulation ischemia who visited the interventional cerebrovascular disease area were included in this study. The treatment effect was observed through abnormal signal changes in the lesion area on each sequence of MRI images before and after treatment. The National Institutes of Health Stroke Scale (NIHSS) was used for the evaluation of the changes in neurological function. *Results*. The real data experiment results suggested that the peak signal-to-noise ratio (PSNR) = 39.33 and structure similarity (SSIM) = 0.96 in the algorithm reconstructed image, which showed no significant difference with the simulation experiment results of PSNR = 35.19 and SSIM = 0.96 ($P < 0.05$). In addition, the stenosis rate after interventional treatment (13.89%) was substantially lower than that before treatment (91.67%) ($P < 0.05$). Cerebral blood flow (CBF) of the bilateral occipital lobes and cerebellum after six months of treatment was higher than that before treatment ($P < 0.05$), and the incidence of postoperative restenosis was 11.11% (4/36). *Conclusion*. The combination of genetic algorithm and compressed sensing algorithm had a good effect on MRI image processing. The posterior circulation ischemia interventional stent implantation can effectively improve the stenosis of the vertebral artery and vertebral basilar artery as well as the cerebral tissue perfusion in the ischemic area, which improved the clinical symptoms substantially and reduced the probability of restenosis.

1. Introduction

Stroke is a common and frequently occurring disease in clinical practice, with a very high rate of disability and mortality, among which ischemic stroke accounts for about 80% [1–3]. About 20% of ischemic stroke cases are caused by posterior circulation ischemia, namely, cerebral ischemia caused by vertebral-basilar artery stenosis, with a mortality rate of about 70% [4]. Clinically, the most common cause of vertebral-basilar stenosis is atherosclerotic plaque. With the development of interventional therapy, intravascular recanalization can improve the prognosis of patients with severe vertebrobasilar artery stenosis or even near occlusion. Studies revealed that early use of endovascular intervention can greatly reduce the incidence of stroke in patients with severe vertebrobasilar artery stenosis, but its safety and effectiveness have not been proven [5]. Compared with the symptoms of anterior circulation ischemia, posterior circulation ischemia has no typical clinical manifestations and imaging characteristics, which is more severe, has higher mortality and longer thrombolytic window, and is easy to cause brain damage. Moreover, the core problem of cerebral ischemia injury is neurological dysfunction caused by neuron damage. To protect and restore the function of

damaged neurons, early treatment and early intervention should be carried out for ischemic brain injury [6, 7]. Therefore, attention should be paid to the early diagnosis and treatment of postcycle ischemic stroke.

A number of studies suggested that the success rate of interventional recanalization in patients with acute cerebral infarction with vertebral basilar stenosis is closely related to the strict screening of patients by imaging techniques [8–10]. Among them, the series of magnetic resonance imaging (MRI) technologies play an important role. However, its imaging speed is slow and susceptible to artifacts, which will affect the diagnostic value of images [11–13]. With the rapid development of science and technology, intelligent algorithm has established a close relationship with medical imaging technology, which, as an auxiliary optimization means, makes the clinical application of medical imaging technology more prominent [14, 15]. Among them, genetic algorithm is a heuristic optimization algorithm that simulates the genetic and evolutionary process of organisms [16]. After many generations of evolution, the fitness of individuals in the population is gradually improved, so as to realize continuous optimization. Compressed sensing can reconstruct high-quality MRI images by means of nonuniform random sampling and using only partial k-space data through sparse constraints and nonlinear algorithms [17].

Therefore, in this study, genetic algorithm was used to screen k-space data which was less affected by motion. MRI image reconstruction using compressed sensing was applied to evaluate the improvement of disease and neurological function of patients with posterior circulation ischemic stroke before and after interventional therapy. It was hoped to provide scientific research basis for rational treatment of posterior circulation ischemic stroke.

2. Methods

2.1. Establishment of Genetic Algorithm and Compression Algorithm to Deal with the MRI Image Artifact Model. In this study, two-dimensional simulation data and real brain magnetic resonance data were used to conduct simulation experiments to prove the feasibility of the algorithm.

2.1.1. Motion Artifact Simulation and Sampling Sequence. In the experiment, each phase encoding in the sampling process is used as the time unit to simulate the movement. Motion includes frequency-encoding direction (FD) translation, phase-encoding direction (PD) translation, and rotation relative to the spatial position of the image at the beginning. The change curve with time is shown in Figure 1, where Figure 1(a) is the clockwise rotation of the head, Figure 1(b) is the patient's movement in the phase-encoding direction, and Figure 1(c) is the patient's movement in the frequency-encoding direction.

Then, Monte Carlo pseudorandom Cartesian sampling mode is adopted, and 15% of the data in the center of k-space is collected first. Based on the energy distribution of the k-space, a pseudorandom sampling sequence is generated through the probability density function (PDF), and the high-frequency part of the k-space is randomly sampled. The PDF format is shown in the following equation:

$$F_x(x) = \int_{-\infty}^{x} f_x(x)\mathrm{d}t. \tag{1}$$

In (1), X is a random variable, $F_x(x)$ is a cumulative distribution function, and $f_x(x)$ is a probability density function.

Finally, random motion simulation is performed according to the above sampling sequence. The original image and the simulated motion artifact image are shown in Figure 2. Figure 2(a) is the still and fully collected BrainWeb image. Figure 2(b) shows that only 30% of the data is still, and Figures 2(c) and 2(d) show the full collection of still data and the full collection of only 40% of the data.

2.1.2. Algorithm Adoption. In MRI technology, the artifact-free signal collected at the position (k_x, k_y) in k-space is expressed as follows:

$$Q\left(k_x, k_y\right) = \int m(x, y)^{-i2\pi\left(k_x x, k_y y\right)}\mathrm{d}x\mathrm{d}y. \tag{2}$$

Since the scanning time in the frequency-encoding direction is very short, the motion in the frequency-encoding direction (k_x direction) is usually ignored, and only the artifacts caused by the motion in the phase-encoding direction (k_y direction) are considered, so the signal containing motion artifacts is expressed as follows:

$$\overline{Q}\left(k_x, k_y\right) = \int m\left(x - r\left(k_y\right), y - t\left(k_x\right)\right)^{-i2\pi\left(k_x x, k_y y\right)}\mathrm{d}x\mathrm{d}y. \tag{3}$$

In (3), $m(x, y)$ is the density distribution function in the image domain space, $r(k_y)$ is the distance moved by the density distribution function in the x direction, and $t(k_x)$ is the distance moved by the density distribution function in the y direction.

The method of removing motion artifacts is divided into the following six steps:

(a) Code chromosome: each bit of each individual's genetic code is initialized, and a value of 0/1 with a 50% probability is randomly assigned.

(b) Estimated fitness value: in this experiment, since there is no reference image for quantitative analysis, the fitness value function is actually a nonreference image quality evaluation function. The nonreference image quality evaluation index QI_{TV} equation is expressed as follows:

$$QI_{\mathrm{TV}} = \frac{\mathrm{TV}_{\mathrm{in}}}{\mathrm{TV}_{\mathrm{out}}}. \tag{4}$$

TV_{in} is the total variation (TV) of the region of interest (ROI) in the reconstructed image, TV_{out} is the total variation of the background region, and ROI is the brain map skull

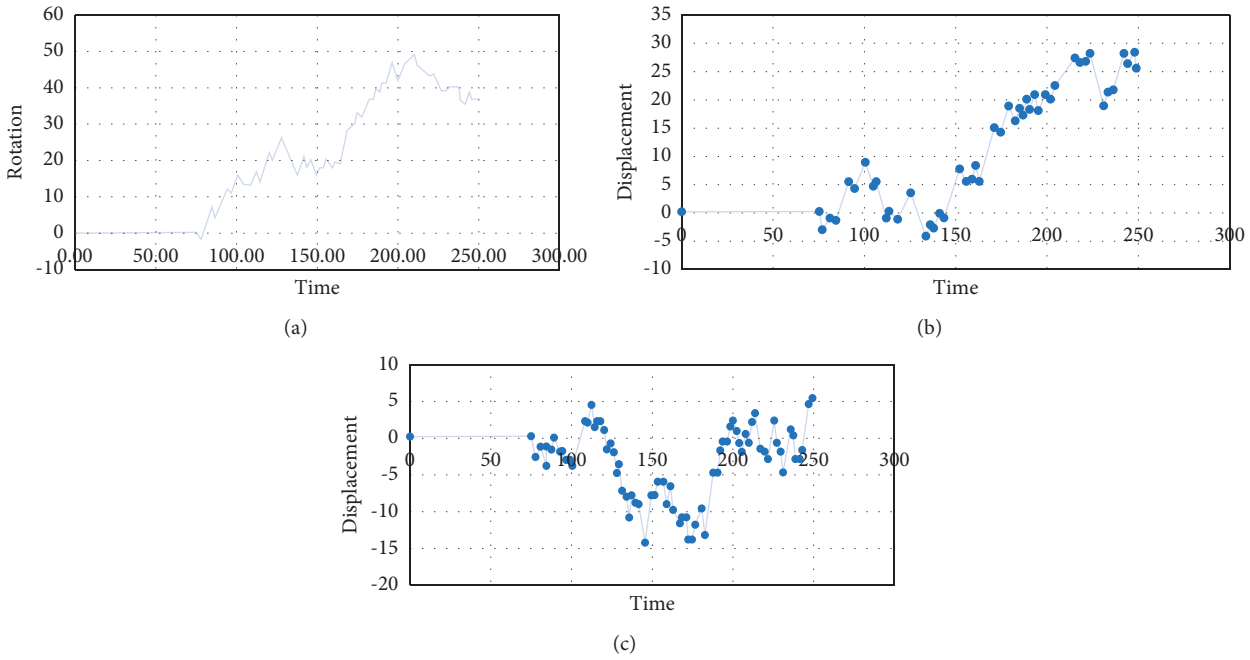

Figure 1: Simulated motion trajectory. (a) Rotation. (b) PD. (c) FD.

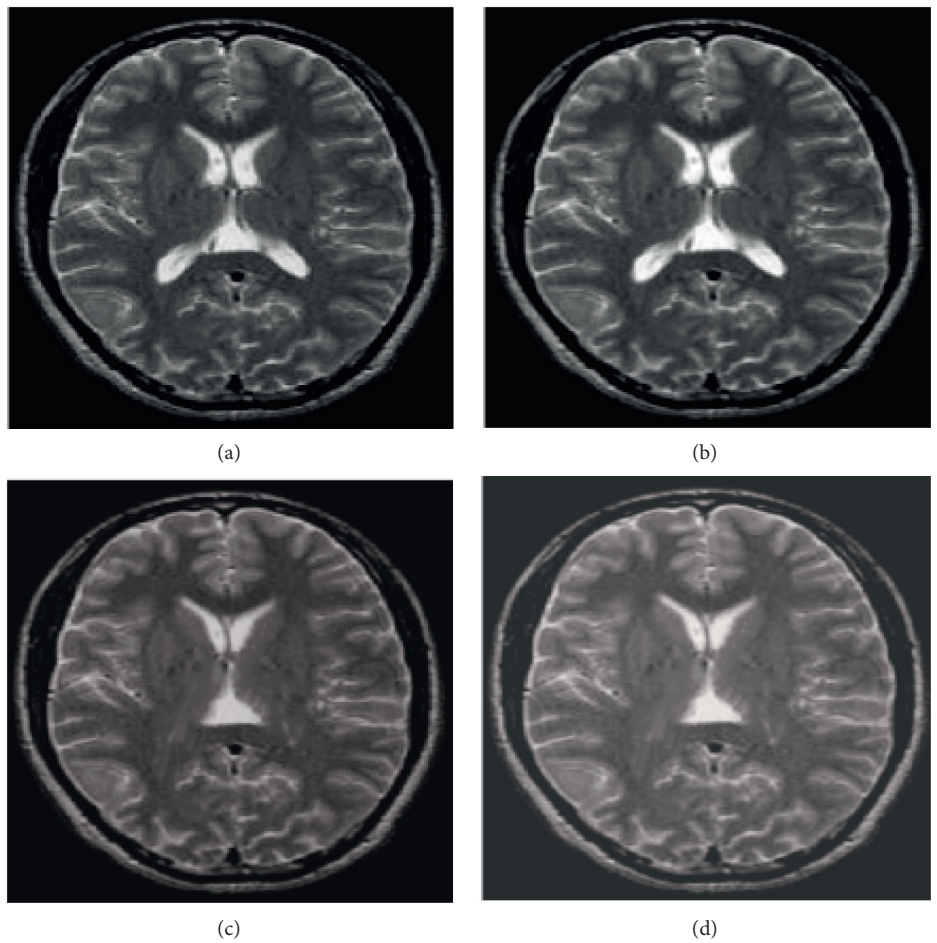

Figure 2: Raw data and simulated motion artifacts. (a) Simulated brain image; (b) simulated brain motion artifact; (c) real brain image; (d) real brain motion artifact.

and its inner region. If the image quality is good, there are few artifacts in the ROI, but it still has certain organizational information. Here, the Otsu algorithm is used to distinguish the ROI from the background, and the expression is as follows:

$$u_{(T)} = w_0 \times u_0 + w_1 + u_1. \tag{5}$$

In (5), w_0 is the proportion of the number of front spots in the image, u_0 is the average gray level, w_1 is the proportion of background points in the image, u_1 is the average gray level, and T is the segmentation threshold between the foreground and the background. When the following (6) is the largest, T is the optimal threshold for segmentation, as shown in Figure 3:

$$\alpha^2 = w_0 \times (u_0 - u_T)^2 + w_1 \times (u_1 - u_T)^2. \tag{6}$$

Due to the large amount of calculation by directly applying the Otsu method, the actual equivalent estimate used is as follows:

$$\alpha^2 = w_0 \times w_1 \times (u_0 - u_1)^2. \tag{7}$$

(c) Selection: the elite strategy is adopted to select the individuals with the top C% of the population, then the championship algorithm is employed to act on all individuals in the population, and the individuals with the population (1-C%) are selected for crossover and mutation operations.

(d) Crossover: the individuals selected by the championship algorithm are crossed with probability of crossover (PC), and the crossover points of individual genes are randomly determined.

(e) Mutation: it is an auxiliary method to generate new individuals, which can avoid the premature convergence of the optimization algorithm. The probability of mutation (PM) is used to perform the inversion operation.

(f) The C% chromosomes selected by the elite strategy are combined with the crossover and mutation (1-C %) chromosomes. The second to sixth steps are repeated until the cycle reaches the specified number of times or the fitness value QI_{TV} no longer increases. The algorithm flowchart is shown in Figure 4.

Each individual is reconstructed by TV-constrained compressed sensing, and its energy function is as follows:

$$X = \operatorname{argmin}_x \|TV(\overline{x})\|_1 + \beta \left\| F_u \overline{x} - y \right\|_2. \tag{8}$$

In (8), β is fidelity parameter.

2.1.3. Evaluation Indexes. The obtained static full-acquisition high-quality images from analog sampling were taken as the gold standard. Two quantitative indicators, peak signal-to-noise ratio (PSNR) and structure similarity (SSIM), were used for the reconstructed image to evaluate the deartifacting effect of the algorithm.

PSNR evaluates the overall image, and SSIM evaluates the structure information of the image from the structural aspect. To prove that QI TV can reflect the quality evaluation index of the reference image, 100 different motion artifact images were randomly generated. Their PSNR and SSIM and those of the gold standard images were calculated, and the correlation between QI_{TV} and the above quantitative indexes were compared.

2.2. Research Objects. A total of 36 cases of posterior circulation ischemia who were treated in the interventional cerebrovascular disease area from August 2019 to November 2020 were included in this study. Among them, there were 22 males and 14 females, aged 45–75 years, with an average of (60 ± 1.28) years. MRI images of patients before and after interventional therapy were divided into two groups. MRI images of patients before and after treatment were processed by genetic algorithm and compressed sensing algorithm. This study had been approved by the Ethics Committee of the hospital, and all patients or their family members signed the informed consent for MRI examination before examination.

Inclusion criteria were as follows: (A) patients with obvious clinical symptoms and complete clinical data, and patients with PCI confirmed by magnetic resonance angiography (MRA) or computerized tomography angiography (CTA) from other hospitals; (B) patients who can cooperate to complete MRI examination, with no contraindication for MR examination; (C) MRI and digital subtraction angiography (DSA) examinations completed within three days; (D) preoperative vertebral basilar artery stenosis ≥70% and confirmed by DSA angiography; (E) patients with adaptation for posterior circulation ischemia interventional therapy; (F) complete and reliable clinical and MRI data before and after interventional treatment.

Exclusion criteria were as follows: (A) patients with anterior circulation stenosis; (B) MRI examination with contraindications; (C) patients allergic to magnetic resonance contrast agent; (D) MRI image quality that was poor and did not meet the diagnostic requirements.

2.3. MRI Scan Methods. The scan sequences of different MRI techniques are shown in Figure 5. The same skilled technician in the department uploaded all the original data to the matching workstation after the scanning was completed. After postprocessing of data and images, image diagnosis analysis was implemented by two experienced physicians in the department, who independently read the images. Accurate recording of various abnormal imaging findings was made, and discussion in case of disputes was made to reach a consensus.

2.4. Interventional Therapy. First, the patient was placed in the supine position, and the patient was given general anesthesia during the operation. After the effect, the patient was routinely disinfected and the towel was laid. Then, the right femoral artery was used as the approach to puncture

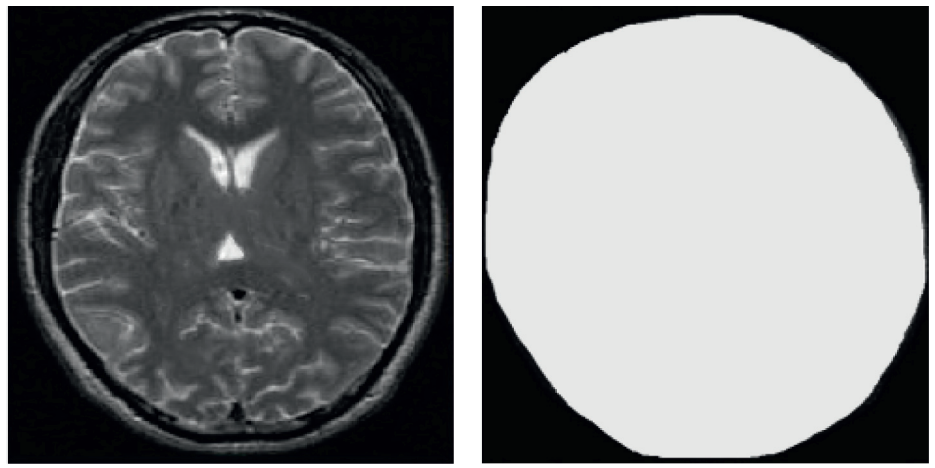

(a) (b)

Figure 3: Example of ROI area in the brain image.

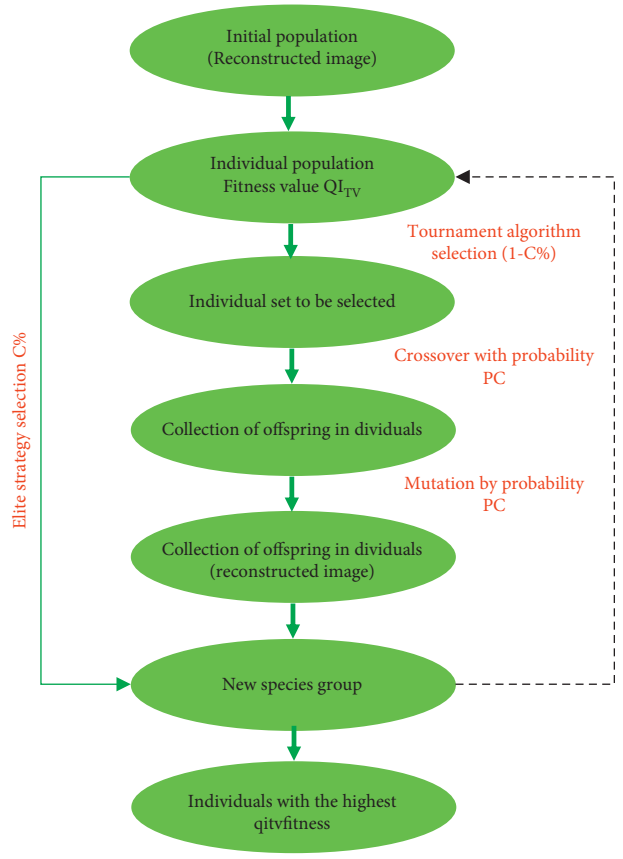

Figure 4: The flowchart of genetic algorithm for image reconstruction.

the 6F artery sheath. The ball guide tube was introduced with the coordination of path diagram and loach guide wire. The catheter tip was placed in place, and angiography showed narrowing of the target artery. Under the path diagram and guided by the microguidewire, the balloon catheter was introduced and placed in the narrowest place. The balloon was expanded, and then the microguidewire and balloon catheter were withdrawn. The microcatheter was placed into the target artery, and the stent was introduced along the microcatheter under fluoroscopy. After the stent was in place, it was released slowly until it was satisfied and adhered to the wall well. Finally, the blood flow improvement of the original stenosis and branch vessels was reviewed by angiography. All operations were successfully completed. All vital signs of the patients were closely observed and timely symptomatic treatment was performed.

Figure 5: MRI scan sequence and pattern.

2.5. Observation Indexes. Abnormal signal changes in different MRI sequences were observed before and after treatment, including vascular stenosis and average cerebral blood flow (CBF) in different brain regions (including bilateral frontal and parietal blood flow in anterior circulation, bilateral occipital and cerebellar blood flow in posterior circulation).

The changes of neurological function were observed before and after treatment. The *National Institutes of Health Stroke Scale* (NIHSS) was used for assessment, which had a total score of 42, and neurological function was inversely proportional to the score [6].

2.6. Statistical Methods. SPSS 22.0 was used for statistical analysis. N (%) was used to represent the enumeration data, and χ^2 test was performed. Shapiro-Wilk W was used to test whether the measurement data complied with the normal distribution. The independent sample t-test was used for rows with normal distribution, and the data were represented by $X \pm S$. The Wilcoxon rank sum test was used for rows with nonnormal distribution, and values were expressed as median (interquartile interval). $P < 0.05$ was considered significant.

3. Results

3.1. Simulated Image Experiment Results. The reconstruction result in the BrainWeb simulation experiment is shown in Figure 6. The proposed genetic algorithm can find most of the k-space data without motion. Among the 30% (80) nonmoving phase-coded data, 77 columns of phase-coded data were found, and 3 columns of nonmoving phase-coded data were omitted. The overall accuracy was 97%. Since most of the data were found, the reconstruction result was similar to the theoretical reconstruction image, which can restore image details and effectively remove motion artifacts. Compared with the theoretical reconstruction image, the PSNR of the obtained reconstructed image was 45.02, and the SSIM = 1. Compared with the gold standard image, the reconstructed image of the algorithm had PSNR = 35.19 and SSIM = 0.96.

3.2. Actual Data Experiment Results. The reconstruction results in the simulation experiment of real brain map motion artifacts are shown in Figure 7. Among 40% (128 columns) of nonmoving phase-encoded data, 127 columns were correctly found, missing 1 nonmoving phase-encoded data column, and 8 more columns of moving phase-encoded data were found. The overall accuracy was 93%. Compared with the theoretical reconstruction image, the PSNR of the reconstructed image obtained was 46.39, and SSIM = 1. Compared with the gold standard image, the reconstructed image of the algorithm had PSNR = 39.33 and SSIM = 0.96.

3.3. Changes of Stenosis Rate in Posterior Circulation Ischemia before and after Interventional Therapy. Of the 36 patients treated with interventional therapy, 12 patients received stents only in the vertebral artery, 20 patients only received stents in the basilar artery, and 4 patients received stents in both the vertebral artery and the basilar artery. The stenosis rate before interventional treatment was 91.67%, which dropped to 13.89% after interventional treatment, and the difference was considerable ($P < 0.05$) (Table 1).

3.4. CBF Changes after Six Months of Treatment. Figure 8 shows the CBF values on the 3D-ASL sequence before treatment and six months of treatment. The CBF of the bilateral occipital lobes and cerebellum after six months of treatment was higher than that before treatment, and the difference was considerable ($P < 0.05$). According to statistics, the probability of restenosis after surgery was 11.11% (4/36). Figure 9 shows the image performance of preoperative MRA, T2WI, T1WI, T2-FLAIR, DWI, SWI, ASL, and

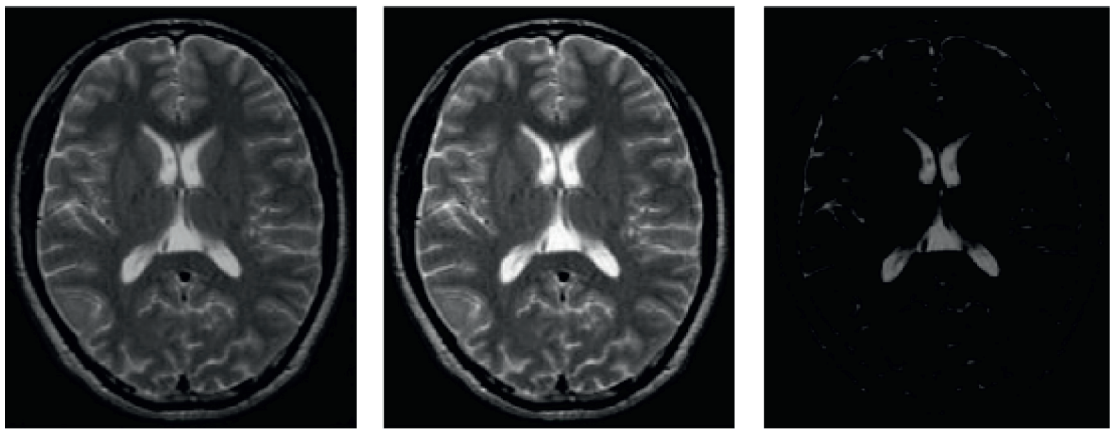

(a) (b) (c)

Figure 6: BrainWeb experiment results. (a) Standard reconstruction image; (b) reconstruction image under the algorithm; (c) contrast image between (a) and (b).

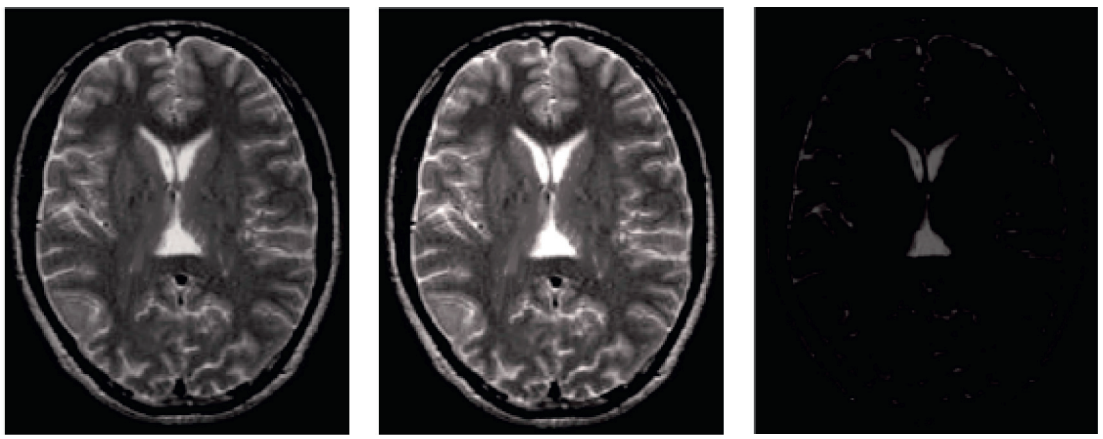

(a) (b) (c)

Figure 7: Experimental results of simulated motion artifacts on actual images. (a) Standard reconstruction image; (b) reconstruction image under the algorithm; (c) contrast image between (a) and (b).

Table 1: Comparison of vascular stenosis between the two groups.

	Stenosis	
	Control group ($n = 36$ cases)	Experimental group ($n = 36$ cases)
Vertebral artery ($n = 12$ cases)	11 (91.67%)	2 (16.67%)*
Basilar artery ($n = 20$ cases)	18 (90.00%)	3 (15.00%)*
Vertebral artery + basilar artery ($n = 4$ cases)	3 (75.00%)	0 (00.00%)*
Total	33 (91.67%)	5 (13.89%)*

Note. The symbol "*" meant that the comparison results were statistically significant ($P < 0.05$).

PWI. The reconstructed image of MRA showed that the lower part of the basilar artery was almost completely occluded. In plain MRI and SWI images, there were no obvious abnormal signals in the planes shown. 3D-ASL images and PWI perfusion images showed no obvious abnormal changes in the planes shown. Figure 10 shows the image performance of MRA, T2WI, T1WI, T2-FLAIR, DWI, SWI, and ASL at six months after surgery, and there were no obvious abnormalities. The PW1 perfusion image showed that the abnormal area of the right cerebellar hemisphere was substantially reduced or even disappeared, indicating that the perfusion was roughly normal.

3.5. Changes in Nerve Function before and after Treatment. Figure 11 shows the neurological function scores of the patients before and after treatment. The neurological function scores of 36 cases of posterior circulation ischemic

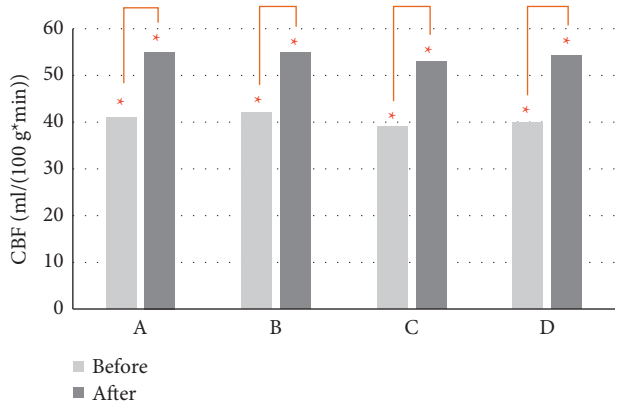

Figure 8: Comparison of CBF values three days before and after intervention. (a) Left occipital lobe; (b) right occipital lobe; (c) left cerebellum; (d) right cerebellum. *Note* The symbol. "*" meant that there was a statistical significance in the comparison results ($P < 0.05$).

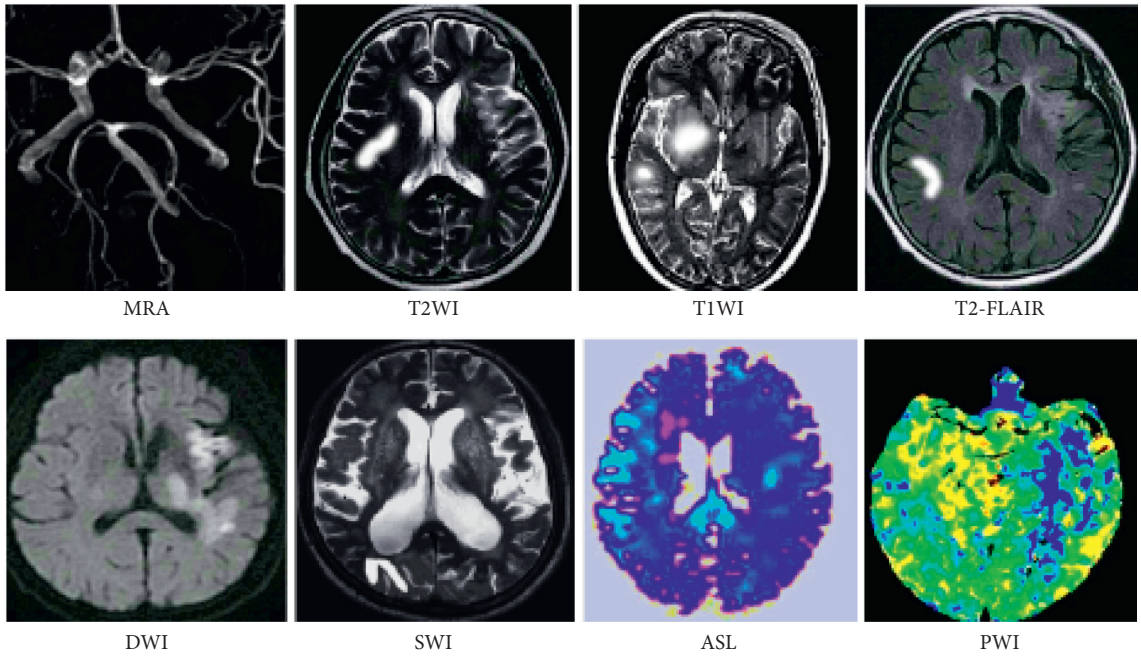

Figure 9: Imaging findings before treatment.

stroke before and after treatment were 34.88 ± 4.12. The neurological function score six months after treatment was 13.23 ± 3.22, and the score before treatment was obviously higher than that after treatment, with substantial differences ($P < 0.05$). Therefore, the neurological function after treatment was better than that before treatment.

4. Discussion

As a common and frequently occurring disease in clinical practice, ischemic stroke poses a great threat to people's health and life, so the effective treatment of this disease has become the focus of research. There is a certain significance of imaging technology for the evaluation of the treatment effect of stroke. Therefore, MRI images processed under genetic algorithm and compressed sensing reconstruction algorithm were introduced to evaluate the improved conditions of patients and neurological function changes before and after interventional treatment.

In this study, genetic algorithm and compressed sensing algorithm were used to reconstruct MRI, and simulation and clinical trials were implemented to verify the effect of this method. The results showed that this method can effectively remove the moving artifacts and improve the image quality. An experimental study using genetic algorithm to correct motion artifacts in MRI images also found that the modified method based on genetic algorithm had a good inhibition effect on artifacts caused by small motion. Compared with the classical iterative algorithm, the inhibition effect on artifacts caused by noise and large motion was greatly improved [18], which was consistent with the results of this study. Of course, genetic algorithm was not only good in

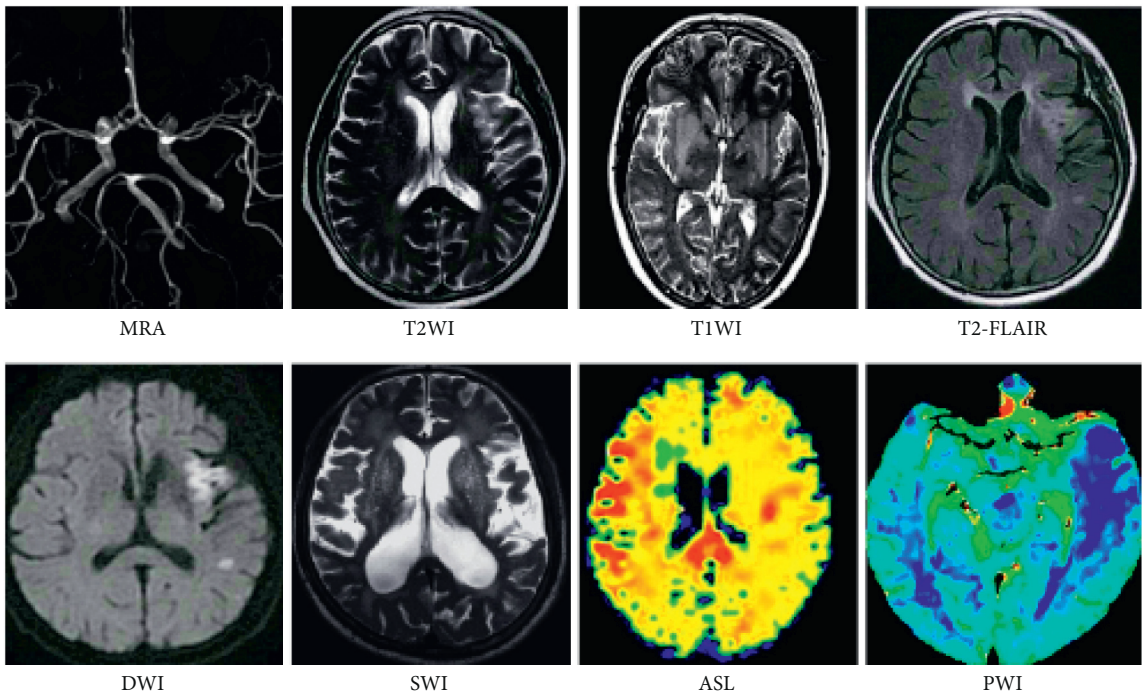

Figure 10: The imaging findings at six months after treatment.

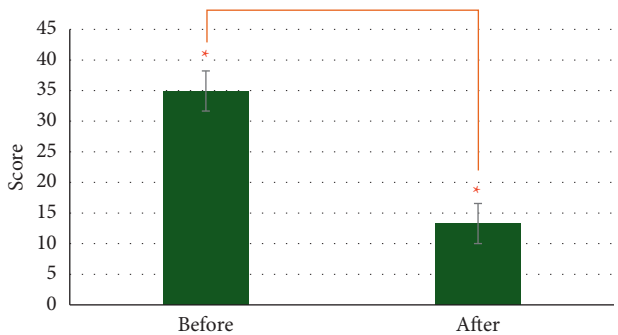

Figure 11: Changes in nerve function before and after treatment. Note: The symbol "*" meant the comparison was of statistical significance ($P < 0.05$).

removing motion artifacts of MRI. Some studies pointed out that genetic algorithm can optimize the segmentation technology of MRI images, making the segmentation reach the accuracy of 92.03%, the specificity of 91.42%, the sensitivity of 92.36%, and the average segmentation score between 0.82 and 0.93. The effectiveness of the proposed technique in identifying normal and abnormal tissues from brain MR images was demonstrated [19]. The above studies all reflected the advantages of genetic algorithm in MRI image processing.

After that, it was applied for the evaluation of the efficacy of interventional treatment on ischemic stroke in the posterior circulation. The results showed that endovascular stent implantation was effective and relatively safe for patients with severe vertebrobasilar stenosis, and the stenosis rate after interventional treatment was significantly lower (13.89% vs 91.67%). The CBF and blood supply were also greatly improved compared with those preoperatively. There was a good short-term curative effect, but the long-term effects remained to be observed in further follow-ups. The short-term efficacy was good, but the long-term results needed to be further followed up. The above results were the same as those of Alexander et al. (2017) [20], who concluded that intravascular treatment of vertebrobasilar atherosclerosis was safe while examining the technical factors that influence the outcome of endovascular treatment for posterior circulation atherosclerotic lesions, especially those of vertebral origin. The reoccurrence rate of stenosis six months after surgery was 11.11%, which was consistent with the results reported that the restenosis rate in stents was 0.06%–43% [21, 22]. It was also concluded that the patients' neurological function was improved significantly after interventional therapy (before treatment vs after treatment: 34.88 ± 4.12 vs 13.23 ± 3.22). This was consistent with the

results of a study on the clinical effect of interventional thrombolysis in patients with acute ischemic stroke and its influence on neurological function [23]. Moreover, it was concluded that, after treatment, neurological function scores of the two groups were decreased and limb function scores were increased, and the experimental group was better than the control group, suggesting that interventional thrombolytic therapy could improve neurological impairment. Besides, more studies have proposed that interventional therapy has a significant effect in the treatment of ischemic stroke in the posterior circulation [24, 25].

5. Conclusion

MRI imaging technology based on genetic algorithm combined with compressed sensing algorithm was used to evaluate the therapeutic effect of endovascular stent intervention on posterior circulation ischemic stroke. The neurological function of the patients before and after interventional therapy was evaluated by NIHSS. It was found that the combination of genetic algorithm and compressed sensing algorithm had a good effect on MRI image processing. The posterior circulation ischemia interventional stent implantation can effectively improve the stenosis of vertebral artery and vertebral basilar artery as well as the cerebral tissue perfusion in the ischemic area, which improved the clinical symptoms substantially and reduced the probability of restenosis. However, the number of subjects in this study is small, and the selected patients are relatively limited, which will lead to the existence of statistical bias. In short, this study can reflect that genetic algorithm has a good application prospect in MRI image processing and stent interventional therapy in the treatment of ischemic stroke caused by posterior circulation stenosis.

Data Availability

The data used to support the findings of this study are available from the corresponding author upon request.

Conflicts of Interest

The authors declare no conflicts of interest.

References

[1] Y. Xing and Y. Bai, "A review of exercise-induced neuroplasticity in ischemic stroke: pathology and mechanisms," *Molecular Neurobiology*, vol. 57, no. 10, pp. 4218–4231, 2020 Oct.

[2] H.-C. Diener and G. J. Hankey, "Primary and Secondary Prevention of Ischemic Stroke and Cerebral Hemorrhage," *Journal of the American College of Cardiology*, vol. 75, no. 15, pp. 1804–1818, 2020 Apr 21.

[3] S. Orellana-Urzúa, I. Rojas, L. Líbano, and R. Rodrigo, "Pathophysiology of ischemic stroke: role of oxidative stress," *Current Pharmaceutical Design*, vol. 26, no. 34, pp. 4246–4260, 2020.

[4] Y. S. Dong, S. L. Xing, H. Y. Zhou, W. Zhang, W. Sun, and J. M. Fan, "[Effects of fast-twisting long-retaining acupuncture therapy on apoptosis and expression of related proteins in vestibular nucleus in rats with vertigo induced by posterior circulation ischemia]," *Zhongguo Zhen Jiu*, vol. 40, no. 2, pp. 179–184, 2020 Feb 12, in Chinese.

[5] Y. Yan, J. Wang, C. Zhong, Y. Zhang, Y. Wei, and H. Liu, "Effects of endovascular stent-assisted angioplasty on cellular metabolism in the Hippocampus of elderly patients with symptomatic vertebrobasilar artery stenosis," *Medical Science Monitor*, vol. 26, Article ID e922131, 2020 May 11.

[6] S. Olivato, S. Nizzoli, M. Cavazzuti, F. Casoni, P. F. Nichelli, and A. Zini, "E-NIHSS: an expanded national Institutes of health stroke Scale weighted for anterior and posterior circulation strokes," *Journal of Stroke and Cerebrovascular Diseases*, vol. 25, no. 12, pp. 2953–2957, 2016 Dec.

[7] T. Dorňák, M. Král, M. Hazlinger et al., "Posterior vs. anterior circulation infarction: demography, outcomes, and frequency of hemorrhage after thrombolysis," *International Journal of Stroke*, vol. 10, no. 8, pp. 1224–1228, 2015 Dec.

[8] P. Khandelwal, D. R. Yavagal, and R. L. Sacco, "Acute ischemic stroke intervention," *Journal of the American College of Cardiology*, vol. 67, no. 22, pp. 2631–2644, 2016 Jun 7.

[9] C. P. Stracke, J. Fiehler, L. Meyer et al., "Emergency intracranial stenting in acute stroke: predictors for poor outcome and for complications," *Journal of the American Heart Association*, vol. 9, no. 5, Article ID e012795, 2020 Mar 3.

[10] E. Siebert, G. Bohner, S. Zweynert et al., "Revascularization Techniques for Acute Basilar Artery Occlusion," *Clinical Neuroradiology*, vol. 29, no. 3, pp. 435–443, 2019 Sep.

[11] R. Bourcier, N. Brecheteau, V. Costalat et al., "MRI quantitative T2∗ mapping on thrombus to predict recanalization after endovascular treatment for acute anterior ischemic stroke," *Journal of Neuroradiology*, vol. 44, no. 4, pp. 241–246, 2017 Jul.

[12] R. G. Sah, C. D. d'Esterre, M. D. Hill et al., "Diffusion-weighted MRI stroke volume following recanalization treatment is threshold-dependent," *Clinical Neuroradiology*, vol. 29, no. 1, pp. 135–141, 2019 Mar.

[13] R. G. González, "Clinical MRI of acute ischemic stroke," *Journal of Magnetic Resonance Imaging*, vol. 36, no. 2, pp. 259–271, 2012 Aug.

[14] Y. Chen, S. Hu, H. Mao, W. Deng, and X. Gao, "Application of the best evacuation model of deep learning in the design of public structures," *Image and Vision Computing*, vol. 102, Article ID 103975, 2020.

[15] X. Gao, S. C. Zhao, and Y. B. Shao, "An Analysis of the Current Status and Countermeasures of Bike-Sharing in the Background of Internet," in *Proceedings of the International Conference on Virtual Reality and Intelligent Systems (ICVRIS)*, Auguest 2018.

[16] D. V. Olson, V. E. Arpinar, and L. T. Muftuler, "Optimization of q-space sampling for mean apparent propagator MRI metrics using a genetic algorithm," *NeuroImage*, vol. 199, pp. 237–244, 2019 Oct 1.

[17] M. Lustig, D. Donoho, and J. M. Pauly, "Sparse MRI: the application of compressed sensing for rapid MR imaging," *Magnetic Resonance in Medicine*, vol. 58, no. 6, pp. 1182–1195, 2007 Dec.

[18] A. Johansson, J. M. Balter, and Y. Cao, "Gastrointestinal 4D MRI with respiratory motion correction," *Medical Physics*, vol. 48, no. 5, pp. 2521–2527, 2021 May.

[19] N. B. Bahadure, A. K. Ray, and H. P. Thethi, "Comparative approach of MRI-based brain tumor segmentation and classification using genetic algorithm," *Journal of Digital Imaging*, vol. 31, no. 4, pp. 477–489, 2018 Aug.

[20] D. Cooke, M. Alexander, J. Rebhun et al., "Technical factors affecting outcomes following endovascular treatment of posterior circulation atherosclerotic lesions," *Surgical Neurology International*, vol. 8, no. 1, p. 284, 2017 Nov 20.

[21] M. K. A. Li, A. C. O. Tsang, F. C. P. Tsang et al., "Long-term risk of in-stent restenosis and stent fracture for extracranial vertebral artery stenting," *Clinical Neuroradiology*, vol. 29, no. 4, pp. 701–706, 2019 Dec.

[22] W. Q. Che, X. J. Jiang, H. Dong et al., "[Effect of stenting for the proximal atherosclerotic extracranial vertebral artery stenosis]," *Zhonghua Xinxueguanbing Zazhi*, vol. 45, no. 1, pp. 34–38, 2017 Jan 25, in Chinese.

[23] S. Majidi, M. Luby, J. K. Lynch et al., "MRI-based thrombolytic therapy in patients with acute ischemic stroke presenting with a low NIHSS," *Neurology*, vol. 93, no. 16, pp. e1507–e1513, 2019 Oct 15.

[24] Y. Yang, C. Liang, C. Shen et al., "The effects of pharmaceutical thrombolysis and multi-modal therapy on patients with acute posterior circulation ischemic stroke: results of a one center retrospective study," *International Journal of Surgery*, vol. 39, pp. 197–201, 2017 Mar.

[25] Q. Huang, H.-q. Song, Q.-f. Ma, X.-w. Song, and J. Wu, "Effects of time delays on the therapeutic outcomes of intravenous thrombolysis for acute ischemic stroke in the posterior circulation: an observational study," *Brain and Behavior*, vol. 9, no. 2, Article ID e01189, 2019 Feb.